

Giant Ly α nebulae associated with high redshift radio galaxies¹

Michiel Reuland^{2,3,4}, Wil van Breugel², Huub Röttgering³, Wim de Vries², S.A. Stanford^{2,4}, Arjun Dey⁵, Mark Lacy⁶, Joss Bland-Hawthorn⁷, Michael Dopita⁸, and George Miley³

ABSTRACT

We report deep Keck narrow-band Ly α images of the luminous $z > 3$ radio galaxies 4C 41.17, 4C 60.07, and B2 0902+34. The images show giant, 100–200 kpc scale emission line nebulae, centered on these galaxies, which exhibit a wealth of morphological structure, including extended low surface brightness emission in the outer regions, radially directed filaments, cone-shaped structures and (indirect) evidence for extended Ly α absorption. We discuss these features within a general scenario where the nebular gas cools gravitationally in large Cold Dark Matter (CDM) halos, forming stars and multiple stellar systems. Merging of these “building” blocks triggers large scale starbursts, forming the stellar bulges of massive radio galaxy hosts, and feeds super-massive black holes which produce the powerful radio jets and lobes. The radio sources, starburst superwinds and AGN radiation then disrupt the accretion process limiting galaxy and black hole growth, and imprint the observed filamentary and cone-shaped structures of the Ly α nebulae.

¹Based on observations made at the W.M. Keck Observatory, which is operated as a scientific partnership among the California Institute of Technology, the University of California and the National Aeronautics and Space Administration. The Observatory was made possible by the generous financial support of the W.M. Keck Foundation.

²Institute of Geophysics and Planetary Physics, Lawrence Livermore National Laboratory, L-413, P.O. Box 808, Livermore, CA 94551 USA, email: mreuland, wil@igpp.ucllnl.org

³Leiden Observatory, P.O. Box 9513, 2300 RA Leiden The Netherlands, email: rottgeri, miley@strw.leidenuniv.nl

⁴Department of Physics, UC Davis, One Shields Avenue, Davis, CA 95616 USA

⁵KPNO/NOAO, 850 N. Cherry Ave., P.O. Box 26732, Tucson, AZ 85726 USA

⁶SIRTF Science Center, Caltech, MS 220-6, 1200 E. California Boulevard, Pasadena, CA 91125 USA

⁷Anglo–Australian Observatory, P.O. Box 296, Epping, NSW 2121 Australia

⁸Research School of Astronomy and Astrophysics, The Australian National University, Cotter Road, Weston Creek, ACT2611, Australia

Subject headings: galaxies: active — galaxies: formation — galaxies: halos — galaxies: high-redshift — galaxies individual: (4C 41.17, 4C 60.07, B2 0902+34) — quasars: emission lines

1. Introduction

High redshift radio galaxies (HzRGs; $z > 2$) are great beacons for pinpointing some of the most massive objects in the early universe, whether these are galaxies, super-massive black holes or even clusters of galaxies (van Breugel et al. 2002).

Powerful, non-thermal radio sources are uniquely associated with massive, multi L_* elliptical galaxies. At *low* redshifts this has been known since the first optical identifications of extra-galactic radio sources were made possible using radio interferometers (Cygnus A; Carilli & Barthel 1996). The large, twin-jet, double-lobe morphologies and enormous radio luminosities ($P_{178\text{MHz}} \sim 5 \times 10^{35} \text{ erg s}^{-1} \text{ Hz}^{-1}$) suggested already early on that such galaxies must have spinning, super-massive black holes (SMBHs) in their centers (Rees 1978; Blandford & Payne 1982). We now know that the masses of the stellar bulges of galaxies and their central black holes are closely correlated ($M_{SMBH} \sim 0.006 M_{bulge}$; Magorrian et al. 1998; Gebhardt et al. 2000; Ferrarese & Merritt 2000), indicating a causal connection and it is no longer a surprise that their parent galaxies occupy the upper end of the galaxy mass function ($\gtrsim 2 \times 10^{11} M_\odot$).

At *high* redshifts the evidence is more recent but equally compelling. The combined near-infrared “Hubble” $K - z$ relation for radio and field galaxies (De Breuck et al. 2002a; Jarvis et al. 2001) shows that radio-loud galaxies are the most luminous at any redshift $0 < z < 5.2$. This is despite considerable changes in their rest-frame morphologies from smooth ellipticals at $z \sim 1$ (Best, Longair, & Röttgering 1998) to large ($\sim 50 - 70$ kpc) multi-component, structures aligned with the radio source at $z > 2$ (Pentericci et al. 1999; van Breugel et al. 1998).

Evidence that the HzRGs are young forming galaxies has been provided by the direct detection of absorption lines and P Cygni-like features from young hot stars (Dey et al. 1997) and strong sub-mm continuum emission (Dunlop et al. 1994; Ivison et al. 1998; Archibald et al. 2001; Reuland et al. 2003a). The sub-mm observations imply “hyper” luminous rest-frame far-infrared luminosities ($L_{FIR} \gtrsim 10^{13} L_\odot$) and huge ($> 1000 M_\odot \text{ yr}^{-1}$) star formation rates (SFRs). Large amounts of star formation are also indicated by the recent detections in several HzRGs of very extended ($\sim 30 - 50$ kpc) molecular gas and dust clouds (Papadopoulos et al. 2000; De Breuck et al. 2002b), showing that the star formation in these systems occurs

on galaxy wide scales.

There are great practical advantages in using HzRGs to study the formation and co-evolution of massive galaxies and their central black holes. Radio source identifications are unbiased with respect to heavy obscuration by dust, which is especially important in young galaxies with large amounts of star formation. Furthermore, HzRGs are the most extended and luminous galaxy-sized structures at many wavelengths and can therefore be studied in great detail over nearly the entire electromagnetic spectrum. Some specific questions that one might hope to address are: Do the stellar bulges of massive elliptical galaxies form mostly during one major, “monolithic” collapse or over a longer period through the merging of smaller components? Does outflow and radiation from starburst and AGN affect the galaxy formation process? Are active, massive forming galaxies capable of enriching the intra-cluster media with metals and thus affect cluster evolution?

It is well established that radio galaxies at low to moderately high redshifts ($z < 2$) often have bright, extended (100 – 200 kpc), emission line nebulae which are aligned with the radio sources (see McCarthy 1993, and references therein). The morphologies, kinematics and ionization of these nebulae have been studied extensively (e.g., van Breugel et al. 1985; Baum, Heckman, & van Breugel 1992; McCarthy 1993; van Ojik et al. 1997; Villar-Martín et al. 1999; Best, Röttgering, & Longair 2000b; Tadhunter et al. 2000; Inskip et al. 2002a). From this work one can conclude that (i) the gas is probably leftover material from earlier galaxy merging events which involve at least one gas rich galaxy, (ii) the kinematics of the gas along the radio source axes is disturbed due to interaction with the radio lobes and jets, (iii) the merging events may have triggered star formation and radio AGN activity at the galaxy centers, and (iv) the gas is ionized in part by shocks induced by the radio sources and in part by photoionization from the AGN (Villar-Martín et al. 1999; Tadhunter et al. 2000; Best, Röttgering, & Longair 2000a,b; Inskip et al. 2002a,b).

Few images exist of extended emission-line ($\text{Ly}\alpha$) nebulae at much higher redshifts ($z > 3$). Most known nebulae are radio-*loud*, being associated with radio galaxies, but some are radio-*quiet* (Steidel et al. 2000; Francis et al. 2001). Nearly all these nebulae were imaged with 4 m class telescopes and little morphological detail can be discerned because of limited signal-to-noise and often moderately poor seeing. Higher quality images are of great interest because of the potential diagnostics they may provide about the very early stages of galaxy formation, and about starburst/AGN feedback and chemical enrichment during this process.

For example, the existence of radio-quiet $\text{Ly}\alpha$ nebulae without obvious central sources of ionization and/or outflow suggests that they may be due to accretion of cooling gas in the gravitational fields of CDM halos (Steidel et al. 2000; Chapman et al. 2001; Fardal et al. 2001; Francis et al. 2001). Such nebulae might be the very first stage in the formation of

large galaxy, or its building blocks, a group of smaller galaxies. The radio-loud Ly α nebulae could be the next phase, during which the central galaxy develops a large scale starburst as a result of galaxy merging and a super-massive black hole is activated. The ensuing outflow and ionizing radiation might then heat and expel the accreting gas, while adding enriched material from the central starburst to the mix, effectively stopping further galaxy growth until starburst and AGN activity subside. Such a self regulated process of galaxy growth has been invoked as a possible explanation for the surprisingly tight SMBH/stellar bulge correlation (Silk & Rees 1998; Haiman & Rees 2001). Could it be that in the case of radio galaxies, which are the most massive systems at any redshift, this process is further aided by radio jets and lobes?

To investigate the nature of Ly α nebulae associated with HzRGs and exploit their diagnostic value we have obtained deep narrow-band Ly α images of three $3 < z < 4$ radio galaxies using the W.M. Keck Observatory 10 m telescopes. Here we discuss the morphologies of these nebulae, their relationship to other pertinent imaging data (radio, infrared, mm), and the possible implications for understanding the formation and coevolution of massive galaxies and super-massive black holes.

Our paper is organized as follows. In Section 2 we describe the target selection, observations and data analysis. The observational results for the individual objects are presented in Section 3 and some physical parameters are deduced. In Section 4, we discuss possible scenarios for the origin of the outer nebulae and the features in the central region. We summarize our conclusions in Section 5. Throughout we adopt a flat universe cosmology with $\Omega_M = 0.3$, $\Omega_\Lambda = 0.7$, and $H_0 = 65 \text{ km s}^{-1} \text{ Mpc}^{-1}$. Note that at the high redshifts of our targets a slightly different choice of cosmological parameters can make a significant difference to the derived parameters. To emphasize this we quote our numbers while retaining the scale factor $h_{65} = 1$. At the redshifts of our galaxies ($z = 3.4 - 3.8$) and using the adopted cosmology we find look-back times $\sim 12.8 h_{65}^{-1} \text{ Gyr}$, galaxy ages $\lesssim 1.7 h_{65}^{-1} \text{ Gyr}$, and angular scales of $\sim 7.6 h_{65}^{-1} \text{ kpc arcsec}^{-1}$.

2. Sample Selection and Observations

The observations presented here include sensitive optical narrow-band and broad-band imaging of three $z > 3$ radio galaxies using the Keck telescopes and previously unpublished Hubble Space Telescope (HST) imaging of 4C 60.07. Our targets were selected on the basis of their high redshifts and the availability of data at many other wavelengths.

2.1. Sample Selection

4C 41.17

4C 41.17 at $z = 3.798$ was chosen because its Ly α halo is one of the most luminous and extended known. Previous imaging observations showed a bright elliptical-shaped Ly α halo with a major axis of $\sim 15''$ directed along the radio axis (Chambers, Miley, & van Breugel 1990; Hippelein & Meisenheimer 1993; Adam et al. 1997; Rocca-Volmerange 1999), and spectroscopic evidence indicated that the Ly α might extend to $\gtrsim 18''$ (Dey 1999). The radio source has a multiple component, asymmetric, “double-double” FR II morphology, with the radio axis of the inner source having a position angle different from the outer source (Chambers, Miley, & van Breugel 1990; Carilli, Owen & Harris 1994). It was the first HzRG in which a large dust mass has been detected through sub-mm observations (Dunlop et al. 1994), implying a large SFR in the range of $2000 - 3000 M_{\odot} \text{yr}^{-1}$.

The galaxy has a clumpy rest-frame UV morphology, with the brightest components aligned with the inner radio source (van Breugel et al. 1999). This light is unpolarized between $\lambda_{\text{rest}} \sim 1400 - 2000 \text{ \AA}$, and thus not due to scattering from a hidden quasar-like AGN (Dey et al. 1997). Instead, the observations show absorption line features from young hot stars which resemble those seen in $z \approx 2 - 3$ star-forming galaxies and nearby starburst systems. Dey et al. derive a SFR of $140 - 1100 M_{\odot} \text{yr}^{-1}$ for the central $10 \text{ kpc} \times 20 \text{ kpc}$ of 4C 41.17 or $400 - 3200 M_{\odot} \text{yr}^{-1}$ after correction for local extinction. These values are consistent with those derived from the sub-mm observations. In this radio source aligned star formation is thought to have been triggered by radio jets colliding with a large, dense cloud in the forming galaxy (Dey et al. 1997; van Breugel et al. 1999; Bicknell et al. 2000).

4C 60.07

4C 60.07 ($z = 3.791$; Chambers et al. 1996) is close to the Galactic plane ($b_{\text{II}} = 12^{\circ}$) and suffers significant Galactic extinction (see, Table 1). Despite this unfortunate circumstance, we selected 4C 60.07 as one of our targets because its redshift is close to that of 4C 41.17 and it is a strong sub-mm emitter and one of only three HzRGs in which CO has been detected (Papadopoulos et al. 2000; De Breuck et al. 2002b). The large extent ($7'' \sim 50h_{65}^{-1} \text{ kpc}$) and dynamical mass ($\sim 1 - 7 \times 10^{11} M_{\odot}$) of the cold gas are some of the best evidence that 4C 60.07 is indeed a massive forming galaxy. A low signal-to-noise image of 4C 60.07 shows a $2''$ Ly α feature aligned with the radio source. The source displays a simple edge brightened FR II morphology (Fanaroff & Riley 1974), unlike the other two objects in our sample (Carilli, Owen & Harris 1994; Chambers et al. 1996).

B2 0902+34

Our third target, B2 0902+34 ($z = 3.395$; Lilly 1988), was selected because of its

extended, very diffuse optical morphology (Eisenhardt & Dickinson 1992), which is very unlike that of the elongated, radio source aligned structures seen in 4C 41.17 and 4C 60.07. It is also the only HzRG for which 21 cm neutral hydrogen has been detected in absorption against the radio continuum (Uson, Bagri, & Cornwell 1991; Briggs, Sorar, & Taramopoulos 1993). No other evidence for cold gas or dust has been found in B2 0902+34. No strong absorption in the Ly α emission has been detected through spectroscopy (Martín-Mirones et al. 1995) and no significant sub-mm signatures of thermal dust emission have been found (Archibald et al. 2001). Eisenhardt & Dickinson (1992) published a shallow Ly α image for B2 0902+34 that showed its halo to be relatively bright but did not reveal much detail. They argued that it is a true protogalaxy, based on its relatively flat UV-optical spectral energy distribution, indicative of a dominant population of young stars. The radio structure resembles that of quasars with a flat spectrum nucleus, a bright knotty jet with a sharp 90° bend in the north, and a disembodied double hotspot to the south. Carilli (1995) explained its unusual properties, inferring that the radio axis is close to the line of sight.

2.2. Keck Imaging

2.2.1. Ly α imaging

We observed 4C 41.17, 4C 60.07 and B2 0902+34 using two custom-made, high throughput narrow-band filters. The central wavelengths and bandpasses were chosen to cover redshifted Ly α within a velocity range of $\pm 1500 \text{ km s}^{-1}$ for each object, which is the typical maximum width of the emission lines of HzRGs (e.g., Dey et al. 1997; van Ojik et al. 1997). 4C 41.17 and 4C 60.07 are close in redshift and fit in the same filter, although for 4C 60.07 emission at velocities larger than 1000 km s^{-1} blueward from the systemic velocity falls outside the bandpass. The transmission curve of this filter ($\lambda_c = 5839.0 \text{ \AA}$ and $\Delta\lambda = 65.0 \text{ \AA}$) averages $\sim 84\%$ over the bandpass. The narrow-band filter for B2 0902+34 has $\lambda_c = 5342.4 \text{ \AA}$ and a FWHM of $\Delta\lambda = 56.8 \text{ \AA}$, with an average transmission of 73%. The fields of view through the $10 \text{ cm} \times 10 \text{ cm}$ filters were vignetted slightly, resulting in an useful sky coverage of $\sim 2'.0 \times 1'.7$.

The observations were made during the nights of UT 2000 December 27, 28 and UT 2001 February 25 using the Echelle Spectrograph and Imager (ESI; Sheinis et al. 2000) at the Cassegrain focus of the Keck II 10 m telescope in imaging mode. The detector used is a high-resistivity MIT-Lincoln Labs 2048×4096 CCD, has a plate scale of $0''.154 \text{ pixel}^{-1}$, and is only partly illuminated in imaging mode. Exposures were broken into integrations of 1200 seconds and we performed $15''$ offsets between each integration. This facilitated removal of cosmic rays and bad pixels on the CCD. The data were taken during photometric

conditions and good seeing (FWHM $0''.6 - 0''.8$ in the co-added images) and were reduced using standard methods in IRAF (including registering and stacking the individual integrations). Flatfielding was done with twilight sky flats only (as opposed to creating field flats from unregistered images) to prevent suppression of faint diffuse emission.

The data were flux calibrated using the spectrophotometric standard stars Feige 34, PG 1121+145, and PG 1545+035 (Massey et al. 1988). All magnitudes and colors quoted in this paper are on the AB system and the individual calibrations agree to within approximately 10%, which we take to be the systematic photometric uncertainty. We corrected for Galactic extinction using the $E(B-V)$ values based upon IRAS $100\mu\text{m}$ cirrus emission maps (Schlegel, Finkbeiner, & Davis 1998) and extrapolating following Cardelli, Clayton, & Mathis (1989). A summary of the total integration times, surface brightness limits, and Galactic extinction corrections is given in Table 1. With 1σ surface brightness limits of $\text{NB} \sim 29 - 30$ mag within an aperture of the seeing disk ($\sim 0.7''$) these are the deepest narrow-band exposures of $\text{Ly}\alpha$ nebulae ever obtained.

2.2.2. Broad-band imaging

We also obtained emission line free R -band images during the same nights to allow continuum subtraction from the narrow-band exposures and create pure $\text{Ly}\alpha$ images. For 4C 41.17 and 4C 60.07 the R -band ($\lambda_c = 6700 \text{ \AA}$; $\text{FWHM} = 1400 \text{ \AA}$) is just redward of $\text{Ly}\alpha$ and free of strong emission lines (all emission lines that fall within the filter bandpass have observed equivalent widths $\lesssim 10 \text{ \AA}$; Dey et al. 1997, Reuland et al. in preparation). In the case of B2 0902+34 the R -band contains the C IV $\lambda\lambda 1548, 1551$ doublet and He II $\lambda 1640$. The spectrum by Martín-Mirones et al. (1995) shows that C IV and He II have observed equivalent widths of $\sim 55 \text{ \AA}$, and $\sim 40 \text{ \AA}$, respectively. The average total contribution of these emission lines to the total flux received in the broad-band filter is $\lesssim 7\%$ indicating that they are only minor contaminants. However, the relative contribution could depend on the region of interest. There is no easy way to correct for this, but compared to the large equivalent width $\text{Ly}\alpha$ line continuum subtraction is only a small correction and does not change any morphological features of interest for this paper. These R -band images have fields of view of $3'.3 \times 1'.7$, were broken into 400s exposures and were reduced following standard methods.

2.3. HST Imaging

4C 60.07 was observed during Cycle 6 with the Wide Field Planetary Camera 2 (WFPC2; Trauger et al. 1994) on the HST. The object was placed on the PC chip, which utilizes an 800×800 pixel Loral CCD as detector with a plate scale of $0''.0455 \text{ pixel}^{-1}$. In two pointings 9 broad-band exposures of 2900s each were obtained for a total exposure time of 26.1 ks through the F702W filter, which has a central wavelength $\lambda_c = 6944.3 \text{ \AA}$ and a FWHM of $\Delta\lambda = 1384.7 \text{ \AA}$. For 4C 60.07 this filter includes the C IV doublet with a combined observed equivalent width of $\sim 300 \text{ \AA}$ (Reuland et al. in preparation), but is free from other strong emission lines. After cosmic ray removal these images were co-added. The data were severely affected by light scattering off of the Earth atmosphere. However, the scattered light pattern was fixed with respect to the CCD. This allowed for using the small offsets between the unregistered images of the two pointings to construct a scattering model. After subtraction of this model, the resulting image was virtually fully corrected.

Deep (21.6 ks) F702W observations of 4C 41.17 were obtained using the PC section of WFPC2 (for details see van Breugel et al. 1999; Bicknell et al. 2000). Observations with the F702W filter are slightly contaminated by the C IV doublet, which has a combined observed equivalent width of $\sim 104 \text{ \AA}$ (Dey et al. 1997).

Eisenhardt and Dickinson observed B2 0902+34 during Cycle 4 for 21.6 ks using the PC of WFPC2 with the filter F622W, which is centered at $\lambda_c = 6189.6 \text{ \AA}$, has a FWHM of $\Delta\lambda = 917.1 \text{ \AA}$, and is free of emission from the Ly α and C IV lines. These data were obtained from the archives.

2.4. Relative Astrometry

Astrometric calibration of the Keck images was performed using the USNO-A2.0 catalog (Monet 1998). For the broad-band images 15 catalog stars were typically available in each field, of which about 10 were unsaturated and suitable for astrometry. In all cases this resulted in astrometry accurate to approximately $0''.15$ rms with respect to the USNO catalog. The catalog itself has a rms uncertainty of $\sim 0''.25$ with respect to the International Celestial Reference Frame (ICRF), while the astrometric uncertainties of the radio images are $\lesssim 0''.2$ with respect to the ICRF (for a concise discussion of relative astrometric uncertainties see De Breuck et al. 2002a, and references therein). The narrow-band image of B2 0902+34 contains only few stars and the astrometry had to be bootstrapped from the broad-band image which has more stars in the field. To do this, the narrow-band image was registered relative to the *R*-band image to better than a fraction of a pixel using a second order polynomial

function. Similarly, the HST images were matched to the respective Keck images resulting in relative optical astrometry better than $0''.1$ rms, and astrometry relative to the radio maps of comparable accuracy as for the Keck imaging.

Generally, for the 5 GHz and 8 GHz VLA radio images (Carilli, Owen & Harris 1994; Carilli 1995; Carilli et al. 1997), we used the astrometry as given by the observations of the phase calibrators. However, in the case of 4C 41.17 there was a faint optical counterpart with a well defined centroid to the serendipitous source to the SE in the 5 GHz map (Source E in Chambers et al. 1996). We used this source to register the radio and optical images to better than $0''.1$. A change of only $+0''.15$ in right ascension and $+0''.2$ in declination was required to align the images. These shifts agree with typical uncertainties in the match between the optical and radio reference frames as cited above. Therefore, we believe that, generally, relative astrometry between the radio and optical is better than $\lesssim 0''.35$ rms, while it is better than $0''.1$ rms in the case of 4C 41.17.

2.5. Continuum subtraction

Pure emission line images were constructed as follows: First, the point spread functions (PSFs) of the narrow-band images were matched to the broader PSFs of the R -band images. For this we selected a suitable star close to the galaxy in both images and calculated a convolution kernel using the IRAF task `psfmatch`. Subsequently, the $\text{Ly}\alpha$ image was convolved with this kernel to obtain a new image with a PSF similar to the R -band image.

The registered R -band images were then divided by a scaling factor, and subtracted from the narrow-band images in order to remove continuum emission. This scaling factor was determined for each radio galaxy by convolving high quality spectra (Dey et al. 1997, Reuland et al. in preparation), after removal of the $\text{Ly}\alpha$ emission line, with the R -band and narrow-band filter curves. For each galaxy this resulted in an expected ratio of continuum flux densities within both filters. These expected ratios are based only on the filter curves, while telescope and CCD efficiencies should be taken into account as well. We corrected for this by adjusting the scaling factor by $\sim 10\%$, which was the difference between the predicted and observed ratios for the spectrophotometric standards.

3. Results

Our narrow-band images show unprecedented detail in the spectacular nebulae that surround the radio galaxies. The nebulae extend over more than 100 kpc and display complex

morphologies such as filamentary structures, conical shapes, and distinct regions of high and low intensity. Grayscale representations (coloreycled to show both low and high surface-brightness regions) of the pure emission line images and contour plots of the narrow-band images (including continuum) are shown in Figures 1–8. In the following, we discuss the morphological features of the nebulae in detail. A summary of their global properties is given in Table 2. This table also gives estimates for the mass of the ionized gas and star formation rates. Despite being subject to considerable uncertainties these might help provide some insight in the nature of the nebulae.

3.1. 4C 41.17

The co-added continuum-subtracted narrow-band image for 4C 41.17 overlaid with a 5 GHz VLA radio map (Carilli, Owen & Harris 1994) is shown in Figure 1, while Figure 2 shows the same image overlaid with a Keck *K*-band image (Graham et al. 1994). Figure 3 shows an overlay of the HST image with the narrow-band image (including continuum). The Ly α nebula is seen to extend over $25'' \times 17''$ ($\sim 190h_{65}^{-1}$ kpc \times $130h_{65}^{-1}$ kpc), nearly twice the size previously seen in the images obtained with 4m class telescopes, and shows a wealth of structure.

Central region

The bright inner region was observed and discussed in detail by Chambers, Miley, & van Breugel (1990). It is aligned with the inner radio source and of approximately the same size, while the radio core is located in a central dip in the Ly α emission. This has been noticed before (Hippelein & Meisenheimer 1993; Adam et al. 1997), and Hippelein & Meisenheimer (1993) interpret the dip as absorption by a foreground Lyman-forest cloud unrelated to the radio galaxy. However, as proposed by Dunlop et al. (1994), it seems more likely that the absorption is due to a dust lane orthogonal to the major axis of the galaxy and its radio source, obscuring the center of the galaxy near the position of the radio core. This would provide a natural explanation for both the observed sub-mm emission and the gap in the UV continuum seen in the HST image (Fig. 3). Graham et al. (1994) also mention that their *K*-band image (Fig. 2; strongly contaminated with [O III] and H β) shows evidence for a double peaked structure. They could not ascertain whether this was also true for a line-free *Ks* image.

Galaxy scale

The Keck *K*-band and HST F702W “R”-band images (rest-frame B-band and 1500Å respectively) show a multi-component galaxy spread out over a region of $9'' \times 5''$ ($\sim 68h_{65}^{-1}$ kpc \times $38h_{65}^{-1}$ kpc) near the center of the Ly α nebula. A Ly α tongue sticks out just SE of the nucleus

and overlaps with continuum emission seen in the Keck and HST images. The HST image shows that this is a small group of kpc-sized clumps, embedded in low surface brightness emission of $\sim 12h_{65}^{-1}$ kpc diameter, which appears to be unaffected by the radio source. From the total UV_{rest} continuum for this region van Breugel et al. (1999) derive a star formation rate of $33 M_{\odot} \text{ yr}^{-1}$ (for the cosmological parameters used in the present paper). For this same region we derive from our Keck observations an integrated Ly α flux of $3 \times 10^{-16} \text{ erg s}^{-1} \text{ cm}^{-2}$, or $L_{\text{Ly}\alpha} = 5 \times 10^{43} \text{ erg s}^{-1}$.

We can convert the Ly α luminosity into an estimate of the star formation rate if we make a few assumptions. With the assumption that all the Ly α is due to Case B recombination of photoionization by stars we obtain $SFR \geq 8.12 \times 10^{-43} f_{\text{esc}}^{-1} L_{\text{Ly}\alpha}$. This assumption, while unlikely to be correct for most of the halo, may be reasonable for the undisturbed region. The estimated SFR constitutes a lower limit as it assumes that a fraction $f_a = 1$ of the ionizing photons will be absorbed. The typical escape fraction found locally is $f_{\text{esc}} \leq 0.1$ (Leitherer et al. 1995). However for the $z \sim 3$ Lyman break galaxy (LBG) population (Steidel et al. 1996) $f_{\text{esc}} \sim 0.5 - 1.0$ is typically found (Steidel, Pettini, & Adelberger 2001) and these LBG values may be more appropriate for HzRGs.

From the inferred $L_{\text{Ly}\alpha}$ we obtain a lower limit to the star formation rate of $40 f_{\text{esc}}^{-1} M_{\odot} \text{ yr}^{-1}$, rather similar to the estimate based on the UV continuum. However, both the UV-continuum and Ly α based SFR estimates are probably lower limits since they assume no extinction, which may very well be important given the detection of dust in 4C 41.17.

Outer region and filamentary structure

Perhaps the most striking morphological feature of the 4C 41.17 Ly α nebula is the cone-shaped structure emanating from the center of the galaxy, with long filaments and a crescent-shaped cloud with horns. The SW outer radio lobe is located within the cone and extends further from the core than its, much fainter, NE counterpart. It suggests that the SW radio lobe may have encountered less dense material on its way out. This also agrees with the emission-line and radio surface brightness asymmetry near the center: the line emission and radio emission of the inner radio source are brighter on the NE side. Such optical/radio asymmetry correlations have also been seen in nearby radio galaxies (McCarthy, Spinrad, & van Breugel 1995). They are thought to be due to local gas density asymmetries, with denser gas blocking radio jets, resulting in brighter line and radio emission.

The filamentary/plume features of the nebula are probably caused by AGN activity and/or the radio source: the long SW filament ($\sim 8''$, $60 h_{65}^{-1}$ kpc) is about the same size as the distance between the nucleus and the SW hotspot, the NE lobe appears to be embraced by two short “plumes” of enhanced Ly α emission, and the apex of the two $\sim 4''$ ($30 h_{65}^{-1}$ kpc) SW cloud horns projects close to the nucleus.

Another point of interest is the *absence* of Ly α emission near several faint K -band companions around 4C 41.17 (Fig. 2; Graham et al. 1994). Based on their red colors ($R - K_s \sim 4 - 5$) Graham et al. concluded that these are probably multiple L_* galaxies at the same redshift as 4C 41.17. Graham’s objects 4, 9 and 12 are all near Ly α “gaps”. It suggests that they are dusty galaxies in the local foreground to the Ly α nebula, absorbing the Ly α photons along the line of sight. If the sizes of the gaps are larger than the K -band objects this could be evidence for galactic envelopes (e.g., Chen, Lanzetta, & Webb 2001). This is hard to test, given the limited signal-to-noise of the K -band objects, but visual inspection of Figure 2 shows that they are consistent with having similar sizes. The scale of the Ly α absorption halos ($15h_{65}^{-1} \text{ kpc} < D < 25h_{65}^{-1} \text{ kpc}$) suggests that these represent objects which have already collapsed to “normal” galaxian dimensions by this redshift.

The 4C 41.17 field also shows an over-density of dusty galaxies on a much larger scale ($\sim 2.5'$ diameter, $\sim 1 h_{65}^{-1} \text{ Mpc}$; Ivison et al. 2000), suggesting that 4C 41.17 may be at the center of a “proto-cluster”.

3.2. 4C 60.07

In Figure 4 we show the continuum-subtracted image of 4C 60.07 overlaid with the 5 GHz VLA radio map of Carilli et al. (1997). Contour overlays of the narrow-band image and 1.25 mm Plateau de Bure map (Papadopoulos et al. 2000) on top of the newly obtained HST image are shown in Figure 5. A zoomed-in version of this HST image with a high resolution 8 GHz VLA map is shown separately in Figure 6 to better bring out the morphological details.

Central region

The radio core appears to fall into a gap in the bright central Ly α emission, and is possibly coincident with a lack of UV continuum emission in the HST images (Figs. 5,6) similar to 4C 41.17. There is enhanced emission on either side of the nucleus, and the Ly α emission is brightest between the nucleus and the eastern lobe which is closest to the nucleus. This emission-line/radio asymmetry correlation is again similar to 4C 41.17 and other radio galaxies.

Galaxy scale

The HST images shown in Figures 5 and 6 show a string of knots subtending at least $5''$ ($\sim 38h_{65}^{-1} \text{ kpc}$). The two brightest knots appear to be on either side of the radio core. There is a prominent Z-shaped structure, both ends of which approximately point toward the radio lobes, making it a typical case of the radio-optical alignment effect. By comparing

the HST morphology with the Ly α emission, it seems that the Z-shaped structure goes around the western peak of the halo (Fig. 5).

Outer region and filamentary structure

On a larger scale the halo extends over approximately $9'' \times 7''$ ($\sim 68h_{65}^{-1}$ kpc \times $53h_{65}^{-1}$ kpc) and shows a cone shaped structure bounded on one side by a $10''$ ($\sim 76h_{65}^{-1}$ kpc) long filament. The maximum projected sizes of the Ly α and radio structures are fairly similar, although the filament extends beyond the radio hotspot by $4''$ ($30h_{65}^{-1}$ kpc). The tip of the filament is co-spatial with a galaxy (Fig. 5). Although it is tempting to infer a connection between the two, spectroscopic observations show that the galaxy is foreground at $z = 0.891$ (Reuland et al. in preparation) and cannot be related. There is also a hint of a filament extending out to the SE.

Interestingly, the mm emission shown in Figure 5 seems almost completely anti-correlated with the Ly α . The Ly α cone and filament appear nearly orthogonal to the cold gas and dust. This morphology seems indicative of an outflow as it resembles luminous starburst galaxies such as M 82. In starburst galaxies this is usually interpreted as being caused by a starburst driven superwind which blows out stellar debris and interstellar gas and dust from the central part of the galaxy (e.g., Strickland & Stevens 2000; Ohyama et al. 2002).

3.3. B2 0902+34

Figure 7 shows the Ly α image and radio map overlay of B2 0902+34. The HST image with narrow-band contours is shown in Figure 8.

Central region

Unlike in 4C 41.17 and 4C 60.07 the central part of the Ly α and continuum emission in B2 0902+34 is not dominated by a high surface brightness elongated, radio-aligned structure. Instead the overall morphology appears more diffuse and bimodal, surrounding the radio core and a curved jet to the north (consistent with Carilli 1995; Pentericci et al. 1999; Fabian, Crawford, & Iwasawa 2002). Figure 8 shows that while there is faint continuum emission to the west co-spatial with the lower luminosity Ly α peak, there seems to be little continuum emission associated with the brightest peak. Dust is not likely to be an important factor in obscuring any continuum on the E, because the Ly α should then be completely extinguished in contrast to the observations and because Archibald et al. (2001) did not find strong signatures of thermal dust emission in the sub-mm. Therefore, the source of ionization in this region remains somewhat unclear, reminiscent of the radio-quiet Ly α halos but with the important distinction that there is a luminous AGN nearby. Given that the

radio axis of the source is oriented close to the line of sight (Carilli 1995), beaming effects are expected to be important. A possibility is that the bright Ly α is due to scattered light from the AGN or the result of collisional excitation. Based on the relatively flat UV-optical spectral energy distribution, Eisenhardt & Dickinson (1992) argued for the presence of a large population of young stars. Both the inner Ly α morphology and the HST continuum might be better understood as being due to a shocked cocoon of gas and possibly shock-induced star formation associated with the approaching radio lobe.

Outer region and filamentary structure

The extended emission line region subtends approximately $10'' \times 8''$ on the sky ($\sim 80h_{65}^{-1}$ kpc \times $64h_{65}^{-1}$ kpc). Again the radio and Ly α structures are roughly comparable in size, and the brightest radio and line emission are on the same side of the core. However, the radio emission near bright Ly α emission is strongly polarized, unlike 4C 41.17 and 4C 60.07. This could be understood if the radio jet in B2 0902+34 is pointed towards us. The shorter line of sight through the gaseous medium would cause less depolarization (the Laing-Garrington effect; Garrington & Conway 1991), and at the same time would boost the core and jet emission due to relativistic beaming.

There are few signs of large scale filamentary emission in B2 0902+34. They could be hidden if the filaments preferentially follow the radio axis and are similarly elongated along our line of sight.

4. Discussion

Our deep, sub-arcsecond seeing narrow-band imaging observations show previously unknown, complex morphologies in giant Ly α nebulae around three HzRGs. Since the nebulae are centered on massive forming galaxies these structures may provide new insights about this galaxy formation process and the importance of starburst/AGN feedback. We will discuss some of the general conclusions that can be drawn from these data. A more in-depth understanding of the nature of the nebulae will require analysis of spectroscopic observations, which will be presented in a following paper. For now we note that these and other spectroscopic evidence for HzRGs show that the nebulae, at least along the *major* axes of the radio sources, are enriched and ionized i.e. are not composed of pure primordial (H, He) gas and not due to Ly α scattering off cold gas (HI). This is based on the detection of C and O along the radio sources over many tens of kpc (e.g., Overzier et al. 2001; Maxfield et al. 2002; van Breugel et al. 2002; Jarvis et al. 2002; Villar-Martín et al. 2002), including evidence for enriched material C IV in undisturbed regions *beyond* radio hotspots (Maxfield et al. 2002; Villar-Martín et al. 2002).

Some of the properties of radio galaxy Ly α nebulae, to the extent that they could be studied with mostly 4 m class telescopes, have been discussed by others (e.g., Chambers, Miley, & van Breugel 1990; Eisenhardt & Dickinson 1992; Hippelein & Meisenheimer 1993; McCarthy 1993; van Ojik et al. 1996, 1997; Rocca-Volmerange 1999; Venemans et al. 2002). Here we will focus on the newly discovered features in our images: the very large low surface brightness outer regions, the long radial filaments and cone-shaped structures, and the (indirect) evidence for extended Ly α absorption. It is important to reiterate that radio-*quiet* Ly α nebulae also exist (Steidel et al. 2000; Francis et al. 2001). It is not known whether the gas in these nebulae is enriched or not, and the available images are of insufficient detail to determine whether they exhibit similar filamentary structures as the HzRG nebulae.

A plausible scenario for explaining the origin of Ly α nebulae is one in which cold gas from the “Dark Ages” is accreted in large Cold Dark Matter halos. In contrast to the classical picture of gas cooling from the virial temperature, $T \sim 10^6$ K for a typical dark matter halo, recent theoretical models predict that most of the infalling gas may not heat to virial temperatures but remains at $T \sim 10^4$ K because of efficient Ly α cooling (Fardal et al. 2001; Haiman, Spaans, & Quataert 2000). There is strong evidence that HzRGs reside in (proto)-clusters (e.g., Pentericci et al. 2000; Venemans et al. 2002), and a viable scenario to explain these nebulae might then be that they are signatures of cooling flows.

As the gas accretes it will condense into stars and galaxies, and thus cooling flow and star formation are intimately linked. The Ly α emission associated with the release of gravitational potential energy is expected to be more spatially extended than emission related to the starburst and they are expected to be of similar magnitude in the most luminous objects (Fardal et al. 2001). The fairly smooth and very extended outer regions orthogonal to the radio sources suggest that these could be the remnants of these initial, undisturbed accretion flows. The surface brightness profile in the outer parts of the SE corner of 4C 41.17, which appears to be the least disturbed part of the nebula, drops off with radius as approximately $I(r) \propto r^{-2}$ and would be consistent with theoretical predictions for cooling halos (Haiman, Spaans, & Quataert 2000).

What about the radial filamentary and cone-shaped structures? How did these form in such a scenario? Here some lessons might be learned from nearby cooling flow clusters, Abell 1795 (Fabian et al. 2001) and NGC 1275 (Conselice, Gallagher, & Wyse 2001; Fabian et al. 2001), starburst superwinds such as in M 82, Arp 220 (e.g., Heckman, Armus, & Miley 1990), and Seyfert II’s (NGC 1068; Dopita et al. 2002).

4.1. Cooling flows and radio lobes

In Abell 1795 there is a long, ~ 80 kpc (projected size), radially directed emission-line and X-ray filament associated with the central cD galaxy. Fabian et al. (2001) consider several possible scenarios to explain this, including a “contrail” induced by ram pressure from the radio source. However, based on kinematic and cooling time considerations, and the fact that the cD galaxy is not quite centered at the X-ray halo, Fabian et al. conclude that the simplest explanation would be that the filament is a cooling wake behind the galaxy as it moves within the X-ray halo. It is possible that the bright, single filament in 4C 60.07 might be explained in this way but we consider this unlikely because of evidence for a very low surface brightness cone-like structure (Fig. 4). The multiple radially directed filaments in 4C 41.17 would also be inconsistent with such a model.

In NGC 1275 numerous radial emission-line filaments are found up to ~ 50 kpc from the central AGN, with some tangential features at large radii. These features overlap with a large radio halo centered on the galaxy. The fairly constant surface brightness along the lengths of the filaments and inferred physical parameters suggest that the filaments formed as a result of compression of the intracluster gas by the expanding radio source (Conselice, Gallagher, & Wyse 2001). The correlation between emission-line and radio source asymmetries in each of the three radio galaxies shows that radio jets and lobes must indeed have a significant impact on the ambient gas emissivity and emission-line morphology. Also, the eastern radio lobe of 4C 41.17 appears to have associated “plumes” of enhanced emission straddling the lobe at both the SW and SE, and the sizes of the radio structures are comparable to those of the emission line gas.

We note that even if the filaments are at a significant distance from the observed radio source components, such as the SW lobe of 4C 41.17, there still is a good reason to believe that they may be causally related, in particular if there is supporting kinematic evidence (see 4C 29.30 for a nearby example; van Breugel et al. 1986). In the canonical picture of radio sources the hotspots and lobes are surrounded by bowshocks and cocoons of radio quiet, shock heated gas with scale sizes which are significantly larger than the observed radio emission (Carilli, Perley, & Dreher 1988; Begelman & Cioffi 1989). The emission-line filaments are then located at the interface of the cocoons and the ambient gas and are not in direct contact with the radio lobes or hotspots and can even extend *beyond* radio hotspots (Figs. 1,4; Maxfield et al. 2002) if one accounts for projection effects and the fact that the radio observations only show the highest surface brightness regions.

4.2. Starburst superwinds

Although HzRGs may not resemble “normal” starburst systems in the strictest sense, it seems reasonable to explore whether galactic superwinds can explain the emission-line morphologies. Observations of low redshift starburst galaxies show weakly collimated bipolar outflows of gas with outflow velocities of several hundred km s^{-1} and up to scales of ~ 10 kpc (Heckman, Armus, & Miley 1990). $\text{H}\alpha$ emission line observations that trace this gas show filaments and arclike structures which are possibly not too dissimilar from the filaments that we can discern in the higher redshift $\text{Ly}\alpha$ nebulae. Spectroscopic evidence for galactic outflows has been found also at high redshifts (e.g., Pettini et al. 1998, 2001; Dawson et al. 2002) from metal absorption lines that are blue-shifted by a few hundred to a few thousand km s^{-1} relative to the estimated systemic velocity of the galaxies. Recent observations of C IV absorptions systems along the lines of sight to QSOs indicate enrichment of the intra-cluster medium (ICM) even at redshifts higher than $z \sim 5$ (Rauch, Sargent, & Barlow 2001) which may have been caused by these outflows.

For a galactic outflow powered by a superwind to occur, the star formation rate per unit area Σ_{SFR} must satisfy the empirical relation $\Sigma_{\text{SFR}} \gtrsim 0.1 \text{ M}_{\odot} \text{ yr}^{-1} \text{ kpc}^{-2}$ (e.g., Heckman 2001). As we have argued above, based on sub-mm detections and direct observations of stellar absorption lines, HzRGs are massive star forming systems, with SFRs of approximately $1000\text{--}2000 \text{ M}_{\odot} \text{ yr}^{-1}$. This implies SFR surface densities of $\Sigma_{\text{SFR}} \gtrsim 0.4 \text{ M}_{\odot} \text{ yr}^{-1} \text{ kpc}^{-2}$ for the regions corresponding to the extent of the K -band (restframe B) continuum. Therefore, the minimum condition for an outflow can be satisfied easily. Similarly, the SFR surface density based on the UV flux and extent of the “undisturbed” southern region in 4C 41.17 $\Sigma_{\text{SFR}} \gtrsim 33 \text{ M}_{\odot} \text{ yr}^{-1} / 100 \text{ kpc}^2 \gtrsim 0.3 \text{ M}_{\odot} \text{ yr}^{-1} \text{ kpc}^{-2}$ would also support a galactic wind.

Models show that starburst outflows fill an over-pressured cavity of hot gas and expand into superbubbles, but they are usually not energetic enough for the bubbles to burst and the gas to escape from the host galaxy (Heckman 2001). This means that for the massive HzRGs this material is likely to reside at large radii but still within the potential well of the galaxy. Taniguchi & Shioya (2000) modelled the outflow of gas and find the following relation for the radii of the shells:

$$r_{\text{shell}} \sim 110 L_{\text{mech},43}^{0.2} n_{\text{H},-5}^{-0.2} t_8^{0.6} \text{ kpc},$$

with $L_{\text{mech}} \sim 10^{43} \text{ erg s}^{-1} \text{ M}_{\odot}^{-1}$ the mechanical luminosity released by supernovae in the starburst, $n_{\text{H},-5}$ the hydrogen density in units of 10^{-5} cm^{-3} and t_8 the age of the starburst in units of 10^8 yr . Dey et al. (1997) modelled the stellar population of 4C 41.17 with a starburst of duration $1.6 \times 10^7 \text{ yr}$ and an older population of stars younger than $6 \times 10^8 \text{ yr}$. This gives a lower and upper limit for t_8 and Chambers, Miley, & van Breugel (1990) estimated $n_{\text{H}} \sim n_e f_v$

with n_e the electron density and f_v the volume filling factor of the clouds to be of order $20 \times 10^{-5} \text{ cm}^{-3}$. Applying these estimates to 4C 41.17 we obtain: $20 \text{ kpc} \leq r_{shell} \leq 170 \text{ kpc}$, resulting in a characteristic extent of the superwind shells $l = 2r_{shell} \sim 150 \text{ kpc}$, consistent with the sizes for the nebulae presented here.

4.3. Radiation pressure driven outflows

Recently, Dopita et al. (2002) presented a model to explain the origin and kinematics of the narrow line regions in Seyfert Galaxies. In this model ionized gas and dust are electrically locked together and streaming from ionization fronts around photo-evaporating clouds located in the ionization cones of the AGN. A similar process might be envisaged in HzRGs. If the dust is destroyed somewhere along the outflow, then the gas will continue to flow outward from the cloud, but radiation pressure will no longer dominate the dynamics. Aguirre et al. (2001) also found that dusty outflows might be radiation pressure driven and can reach distances of up to a few 100 kpc. These models suggest that radiative ablation by the central source may be a significant if not dominant contributor to outflows.

Such a scenario would explain why the filaments are all oriented radially, and why the focal point of the tails of the SW emission line cloud in 4C 41.17 seems to be the radio core while there is no obvious connection with the radio emission.

4.4. Obscured AGN

For all three galaxies in the sample, and for 4C 23.56 which was extensively studied by Knopp & Chambers (1997), the radio core appears to be located in a hole or at least a depression in the bright central part of the $\text{Ly}\alpha$ line emission. The best example of this is 4C 41.17 where the UV continuum also shows a gap of approximately $0''.4$ ($\sim 3h_{65}^{-1} \text{ kpc}$). Because the dips are also apparent in the UV continuum and because there appears to be very bright emission on either side, the gap must be due to an obscuring medium of high optical depth. MRC 1243+036 is the only HzRG with a well studied $\text{Ly}\alpha$ halo for which the radio core appears associated with a peak in $\text{Ly}\alpha$ (van Ojik et al. 1996). However, the central shape of MRC 1243+036 bears close resemblance to the central cone shapes of 4C 60.07, and it is quite possible that the central region would show two distinct components with the radio core being in between if it were observed at higher resolution.

Hippelein & Meisenheimer (1993) were the first to notice the gap in the $\text{Ly}\alpha$ image of 4C 41.17 and interpreted it as being due to a foreground absorber being part of the $\text{Ly}\alpha$

forest. The strong sub-mm dust detection of 4C 41.17 led Dunlop et al. (1994) to speculate that this gap might rather be due to a dusty disk. While this remains a viable option, in the case of 4C 60.07 which shows a similar UV continuum and emission line dip, sub-mm observations show that *most* of the dust is located “outside” the galaxy.

At least two of the three radio galaxies that we present here, show a distinct biconical shape in the brightest parts of their nebulosities. This morphology suggests that the nucleus contributes significantly to the photoionization, and is surrounded by an obscuring torus which we observe under an angle as favored by the quasar-radio galaxy unification scheme (Barthel 1989). This putative torus would be much larger than what is traditionally assumed and it would be more appropriate to refer to this feature as a dust lane. Dust lanes have been studied in nearby FR I radio galaxies (Verdoes Kleijn et al. 1999), and appear to be orthogonal to the radio axis independent of the orientation of the galactic disk. Verdoes et al. found that these features typically range from 200 pc to 4.5 kpc, while features larger than ~ 1 kpc show peculiar morphologies and are possibly still settling towards stable orbits. This suggests that the large sizes seen in HzRGs might be the result of the availability of substantial amounts of debris and that the torus/dust lane is still forming and has not yet reached its final configuration.

5. Conclusions

We have presented a morphological study of the Ly α emission line nebulae of three radio galaxies at redshifts $z \sim 3.4 - 3.8$.

Our new findings are that the emission line nebulae show giant, 100 - 200 kpc low surface brightness emission and large (up to 80 kpc) filamentary and cone-shaped structures, which are even more extended than known previously. We have also found indirect evidence for extended Ly α absorption due to neighboring galaxies in the local foreground to the 4C 41.17 nebula and, in all three cases, that the AGN appear obscured by surrounding dust.

In order to explain these observations, we have presented a scenario in which primordial cooling flows in Cold Dark Matter halos form multiple stellar systems which merge, building the stellar bulges of future massive galaxies and triggering (radio-loud) SMBH activity. The radio jets, starburst superwinds and radiative ablation from the AGN may all contribute to cause the observed radially directed filamentary structures, in at least two of the three objects studied, and may provide a feedback mechanism which regulates stellar bulge and SMBH growth. To study these processes will require further observations of the physical properties of the gas, and numerical simulations of the effects of jets and AGN radiation on

dusty, astrophysical plasmas. Some regions of the outermost halos appear unaffected by any radio/AGN activity. This suggests that this gas must either be infalling for the first time or be a remnant of previous outflows.

Deep spectroscopy targeting non-resonant emission lines are important to constrain the various scenarios, and determine the gas kinematics, metallicities and sources of ionization. The observations presented here also show that filamentary structure is not always aligned with the radio axis, and that long slit spectroscopy can easily miss large, bright filaments. Therefore, to fully exploit narrow-band emission-line images as a tool for studies of galaxy formation requires the use of “3-Dimensional” (2-D spatial + 1-D spectral) imaging devices on large telescopes (van Breugel & Bland-Hawthorn 2000). Several such devices are currently being build, including the LLNL Imaging Fourier Transform Spectrometer (Wurtz et al.2001), and the OSIRIS imaging spectrograph for the Spanish 10.4 m telescope GTC at La Palma (Cepa et al.2001).

It is a pleasure to thank Chris Carilli for making available the VLA radio maps, Padeli Papadopoulos for providing us with the PdB images, Björn Heijligers for IDL tips and tricks, and the staff at W.M. Keck Observatory for their efficient assistance. We thank the referee, Montse Villar-Martín for many helpful suggestions that improved the manuscript. The work of M.R., W.d.V., W.v.B., A.S., and M.L. was performed under the auspices of the U.S. Department of Energy, National Nuclear Security Administration by the University of California, Lawrence Livermore National Laboratory under contract No. W-7405-Eng-48. W.v.B. also acknowledges NASA grants GO 5429, 5765, 5940, 6608, and 8183 in support of HzRG research with HST at LLNL. M.L. performed part of this work at the Jet Propulsion Laboratory, California Institute of Technology, under contract with NASA. M.D. acknowledges the support of the ANU and the Australian Research Council (ARC) for his ARC Australian Federation Fellowship, and also under the ARC Discovery project DP0208445. This research has made use of the USNOFS Image and Catalogue Archive operated by the United States Naval Observatory, Flagstaff Station (<http://www.nofs.navy.mil/data/fchpix/>), and the NASA/IPAC Extragalactic Database (NED) which is operated by the Jet Propulsion Laboratory, California Institute of Technology, under contract with the National Aeronautics and Space Administration.

REFERENCES

- Adam, G., Rocca-Volmerange, B., Gérard, S., Ferruit, P. & Bacon, R., 1997, *A&A*, 326, 501
Aguirre, A., Hernquist, L., Schaye, J., Katz, N., Weinberg, D.H. & Gardner, J., 2001, *ApJ*,

561, 521

- Archibald, E.N., Dunlop, J.S., Hughes, D.H., Rawlings, S., Eales, S.A. & Ivison, R.J., 2001, MNRAS, 323, 417
- Barthel, P.D., 1989, ApJ, 336, 606
- Baum, S.A., Heckman, T.M., & van Breugel, W., 1992, ApJ, 389, 208
- Begelman, M. C. & Cioffi, D. F. 1989, ApJ, 345, L21
- Bertin, E. & Arnouts, S., 1996, A&A, 117, 393
- Best, P.N., Longair, M.S. & Röttgering, H.J.A., 1998, MNRAS, 295, 549
- Best, P. N., Röttgering, H. J. A., & Longair, M. S. 2000a, MNRAS, 311, 1
- Best, P. N., Röttgering, H. J. A., & Longair, M. S. 2000b, MNRAS, 311, 23
- Bicknell, G., Sutherland, R., van Breugel, W., Dopita, M., Dey, A. & Miley, G. 2000, ApJ, 540, 678
- Binette, L., Kurk, J. D., Villar-Martín, M., & Röttgering, H. J. A. 2000, A&A, 356, 23
- Blandford, R. D. & Payne, D. G. 1982, MNRAS, 199, 883
- Briggs, F. H., Sorar, E. & Taramopoulos, A., 1993, ApJ, 415, L99
- Cardelli, J.A., Clayton, G.C. & Mathis, J.S. 1989, ApJ, 345, 245
- Carilli, C. L., Perley, R. A., & Dreher, J. H. 1988, ApJ, 334, L73
- Carilli, C.L., Owen, F.N. & Harris, D.E. 1994, AJ, 107, 480
- Carilli, C.L., 1995, A&A, 298, 77
- Carilli, C. L. & Barthel, P. D. 1996, A&A Rev., 7, 1
- Carilli, C.L., Röttgering, H.J.A., van Ojik, R., Miley, G.K. & van Breugel, W.J.M. 1997, ApJ, 109, 1
- Cepa, J., González-Serrano, J. I., & del Río, M. S. 2001, The Promise of the Herschel Space Observatory. Eds. G.L. Pilbratt, J. Cernicharo, A.M. Heras, T. Prusti, & R. Harris. ESA-SP 460, p. 373, 460, 373
- Chambers, K.C., Miley, G.K. & van Breugel, W.J.M., 1990, ApJ, 363, 21

- Chambers, K.C., Miley, G.K., van Breugel, W.J.M., Bremer, M.A.R., Huang, J.S. & Trentham, N.A. 1996, *ApJS*, 106, 247
- Chapman, S.C., Lewis, G.F., Scott, D., Richards, E., Borys, C., Steidel, C.C., Adelberger, K.L., & Shapley, A.E., 2001, *ApJ*, 548, L17
- Chen, H-W., Lanzetta, K. & Webb, J. 2001, *ApJ*, 556, 158
- Conselice, C. J., Gallagher, J. S., & Wyse, R. F. G. 2001, *AJ*, 122, 2281
- Dawson, S., Spinrad, H., Stern, D., Dey, A., van Breugel, W., de Vries, W. & Reuland, M., 2002, *ApJ*, 570, 92
- De Breuck, C., van Breugel, W., Stanford, S.A., Röttgering, H., Miley, G. & Stern, D., 2002a, *AJ*, 123, 637
- De Breuck, C. et al., 2002b, submitted.
- Dey, A., van Breugel, W., Vacca, W.D. & Antonucci, R., 1997, *ApJ*, 490, 698
- Dey, A., 1999, in *Proc. KNAW Colloq.* 49, 19
- Dopita, M.A., Groves, B.A., Sutherland, R.S., Binette, L. & Cecil, G., 2002, *astro-ph/0203360*
- Dunlop, J. S., Hughes, D. H., Rawlings, S., Eales, S. A., & Ward, M. J., 1994, *Nature*, 370, 347
- Eisenhardt, P. & Dickinson, M., 1992, *ApJ*, 399, L47
- Fabian, A. C., Sanders, J. S., Ettori, S., Taylor, G. B., Allen, S. W., Crawford, C. S., Iwasawa, K., & Johnstone, R. M. 2001, *MNRAS*, 321, L33
- Fabian, A. C., Crawford, C. S. & Iwasawa, K., 2002, *MNRAS*, 331, L57
- Fanaroff, B. L. & Riley, J. M. 1974, *MNRAS*, 167, 31P
- Fardal, M. A., Katz, N., Gardner, J. P., Hernquist, L., Weinberg, D. H., & Davé, R., 2001, *ApJ*, 562, 605
- Ferrarese, L. & Merritt, D., 2000, *ApJ*, 539, L9
- Francis, P. J. et al. 2001, *ApJ*, 554, 1001
- Garrington, S.T. & Conway, R.G., 1991, *MNRAS*, 250, 198

- Gebhardt, K. et al., 2000, *ApJ*, 539, 13
- Graham, J. R. et al., 1994, *ApJ*, 420, L5
- Haiman, Z., Spaans, M. & Quataert, E., 2000, *ApJ*, 537, L5
- Haiman, Z. & Rees, M.J., 2001, *ApJ*, 556, 87
- Heckman, T. M., Miley, G. K., Balick, B., van Breugel, W. J. M., & Butcher, H. R. 1982, *ApJ*, 262, 529
- Heckman, T. M., Armus, L., & Miley, G. K. 1990, *ApJS*, 74, 833
- Heckman, T.M., 2001, astro-ph/0107438
- Hippelein, H. & Meisenheimer, K., 1993, *Nature*, 362, 224
- Inskip, K. J., Best, P. N., Rawlings, S., Longair, M. S., Cotter, G., Röttgering, H. J. A., & Eales, S. 2002a, *MNRAS*, accepted, astro-ph/0208548
- Inskip, K. J., Best, P. N., Röttgering, H. J. A., Rawlings, S., Cotter, G., & Longair, M. S. 2002b, *MNRAS*, accepted, astro-ph/0208549
- Iverson, R. J. et al. 1998, *ApJ*, 494, 211
- Iverson, R.J., Dunlop, J.S., Smail, I., Dey, A., Liu, M.C. & Graham, J.R., 2000, *ApJ*, 542, 27
- Jarvis, M. J., Rawlings, S., Eales, S., Blundell, K. M., Bunker, A. J., Croft, S., McLure, R. J., & Willott, C. J. 2001, *MNRAS*, 326, 1585
- Jarvis, M. J., Wilman, R.J, Röttgering, H.J.A & Binette, L., 2002, *MNRAS*, accepted
- Knopp, G.P. & Chambers, K.C. 1997, *ApJS*, 109, 367
- Leitherer, C., Ferguson, H. C., Heckman, T. M., & Lowenthal, J. D. 1995, *ApJ*, 454, L19
- Lilly, S.J., 1988, *ApJ*, 333, 161
- Magorrian, J. et al., 1998, *AJ*, 115, 2285
- Martín-Mirónes, J.M., Martínez-González, E., González-Serrano, J.I. & Sanz, J.L., 1995, *ApJ*, 440, 191
- Massey, P., Strobel, K., Barnes, J.V. & Anderson, E., 1988, *ApJ*, 328, 315
- Maxfield, L., Spinrad, H., Stern, D., Dey, A., & Dickinson, M. 2002, *AJ*, 123, 2321

- McCarthy, P. J., Spinrad, H., Dickinson, M., van Breugel, W., Liebert, J., Djorgovski, S., & Eisenhardt, P. 1990, *ApJ*, 365, 487
- McCarthy, P. J., 1993, *ARA&A*, 31, 639
- McCarthy, P. J., Spinrad, H., & van Breugel, W. 1995, *ApJS*, 99, 27
- Monet, D. G. 1998, American Astronomical Society Meeting, 193, 112003
- Ohyama, Y. et al. 2002, astro-ph/0209442
- Overzier, R. A., Röttgering, H. J. A., Kurk, J. D., & De Breuck, C. 2001, *A&A*, 370, L39
- Papadopoulos, P.P., Röttgering, H.J.A., van der Werf, P.P., Guilloteau, S., Omont, A., van Breugel, W.J.M. & Tilanus, R.P.J., 2000, *ApJ*, 528, 626
- Pentericci, L., Röttgering, H.J.A., Miley, G.K., McCarthy, P., Spinrad, H., van Breugel, W.J.M. & Macchetto, F., 1999, *A&A*, 341, 329
- Pentericci, L. et al. 2000, *A&A*, 361, L25
- Pettini, M., Kellogg, M., Steidel, C., Dickinson, M., Adelberger, K. & Giavalisco, M., 1998, *ApJ*, 508, 539
- Pettini, M., Shapley, A.E., Steidel, C.C., Cuby, J., Dickinson, M., Moorwood, A.F.M., Adelberger, K.L. & Giavalisco, M., 2001, *ApJ*, 554, 981
- Rauch, M., Sargent, W. L. W., & Barlow, T. A. 2001, *ApJ*, 554, 823
- Rees, M. J. 1978, *Nature*, 275, 516
- Reuland, M. et al. submitted
- Rocca-Volmerange, B. 1999, *The Most Distant Radio Galaxies*, 245
- Schlegel, D.J., Finkbeiner, D.P. & Davis, M., 1998, *ApJ*, 500, 525
- Sheinis, A.I., Miller, J.M., Bolte, M. & 2000, *Proc. SPIE*, 4008, 522
- Silk, J. & Rees, M. J. 1998, *A&A*, 331, L1
- Steidel, C.C., Giavalisco, M., Pettini, M., Dickinson, M. & Adelberger, K.L. 1996, *ApJ*, 462, L17
- Steidel, C. C., Adelberger, K. L., Shapley, A. E., Pettini, M., Dickinson, M., & Giavalisco, M. 2000, *ApJ*, 532, 170

- Steidel, C. C., Pettini, M., & Adelberger, K. L. 2001, *ApJ*, 546, 665
- Strickland, D. K. & Stevens, I. R., 2000, *MNRAS*, 314, 511
- Tadhunter, C. N., Villar-Martin, M., Morganti, R., Bland-Hawthorn, J., & Axon, D. 2000, *MNRAS*, 314, 849
- Taniguchi, Y. & Shioya, Y. 2000, *ApJ*, 532, L13
- Trauger, J. T. et al. 1994, *ApJ*, 435, L3
- Uson, J. M., Bagri, D. S., & Cornwell, T. J. 1991, *Physical Review Letters*, 67, 3328
- van Breugel, W., Miley, G., Heckman, T., Butcher, H. & Bridle, A., 1985, *ApJ*, 290, 496
- van Breugel, W. J. M., Heckman, T. M., Miley, G. K. & Filippenko, A. V., 1986, *ApJ*, 311, 58
- van Breugel, W.J.M., Stanford, S.A., Spinrad, H., Stern, D. & Graham, J.R., 1998, *ApJ*, 502, 614
- van Breugel, W. et al. 1999 in *Proc. KNAW Colloq.* 49, 49
- van Breugel, W. & Bland-Hawthorn, J. 2000, *PASP*, 112, 579
- van Breugel, W. et al. 2002, *astro-ph/0209173*
- van Ojik, R., Röttgering, H.J.A., Carilli, C.L., Miley, G.K., Bremer, M.N. & Macchetto, F., 1996, *A&A*, 313, 25
- van Ojik, R., Röttgering, H.J.A., Miley, G.K. & Hunstead, R.W., 1997, *A&A*, 317, 358
- Venemans, B. P. et al. 2002, *ApJ*, 569, L11
- Verdoes Kleijn, G. A., Baum, S. A., de Zeeuw, P. T., & O’Dea, C. P. 1999, *AJ*, 118, 2592
- Vernet, J., Fosbury, R. A. E., Villar-Martín, M., Cohen, M. H., Cimatti, A., di Serego Alighieri, S., & Goodrich, R. W. 2001, *A&A*, 366, 7
- Villar-Martín, M., Tadhunter, C., Morganti, R., Axon, D., & Koekemoer, A. 1999, *MNRAS*, 307, 24
- Villar-Martín, M., Vernet, J, di Serego Alighieri, S., Fosbury, R., Pentericci, L., Cohen, M., Goodrich, R. & Humphrey, A., 2002, *MNRAS*, accepted, *astro-ph/0206118*

Wurtz, R., Wishnow, E., Blais-Ouellette, S., Cook, K., Carr, D., Grandmont, F., Lewis, I.
& Stubbs, C., 2001, *Galaxies: the Third Dimension*. Eds. M. Rosado, L. Binette, L.
Arias, ASP Conf. Ser, astro-ph/0203501

Table 1. Summary of Keck observations

Object	Coordinates ^a		Narrow-band			R-band	
	RA (J2000)	DEC (J2000)	Gal.Ext. ^b mag	t_{obs} (ks)	1σ det.surf.br. ^c (AB mag)	t_{obs} (ks)	1σ det.surf.br. ^c (AB mag)
B2 0902+34	09 05 30.11	34 07 55.9	0.101	9.6	29.04, 27.4	2.4	29.70, 28.3
4C 60.07	05 12 55.17	60 30 51.1	1.609	7.2	28.85, 27.3	2.0	29.64, 28.1
4C 41.17	06 50 52.14	41 30 30.7	0.393	27.6	29.85, 28.1	4.0	30.08, 28.7

^aPosition of the radio core (Carilli, Owen & Harris 1994; Carilli et al. 1997; Carilli 1995)

^bGalactic extinction at the central wavelength of the narrow-band filters

^cFormal 1σ detection limit: in the seeing disc and in a $3''$ diameter aperture respectively

Table 2. Properties of the Ly α nebulae

Object	z	NB ^a mag	BB–NB mag	$F_{\text{Ly}\alpha}$ ^b $\text{erg s}^{-1} \text{cm}^{-2}$	$\log L_{\text{Ly}\alpha}$ ^c erg s^{-1}	Extent " \times "	Size ^c kpc \times kpc	Mass ^d $10^8 M_{\odot}$	SFR ^e $M_{\odot} \text{ yr}^{-1}$
B2 0902+34	3.395	19.20 ± 0.004	2.81	4.9×10^{-15}	44.77	10 \times 8	80 \times 64	$30 f_{\text{v}}^{-\frac{1}{2}}$	$> 450 f_{\text{esc}}^{-1}$
4C 60.07	3.791	19.97 ± 0.050	3.26	8.8×10^{-15}	45.14	9 \times 7	68 \times 53	$30 f_{\text{v}}^{-\frac{1}{2}}$	$> 1100 f_{\text{esc}}^{-1}$
4C 41.17	3.798	18.76 ± 0.001	3.38	9.0×10^{-15}	45.15	25 \times 17	190 \times 130	$130 f_{\text{v}}^{-\frac{1}{2}}$	$> 1100 f_{\text{esc}}^{-1}$

^aDetermined using SExtractor (Bertin & Arnouts 1996) with automatic aperture selection and deblend parameter optimized for detecting large structures. The uncertainties quoted are the formal error estimates given by SExtractor. The magnitudes were also determined in IRAF using a curve of growth for the cumulative magnitude in increasing radii which resulted in magnitudes differing by at most 0.3 mag.

^bCorrected for Galactic extinction

^cAssuming a cosmology with $\Omega_{\text{M}} = 0.3$, $\Omega_{\Lambda} = 0.7$, and $H_0 = 65 \text{ km s}^{-1} \text{ Mpc}^{-1}$

^dThese mass estimates are derived from $M = n_e m_p f_{\text{v}} V$ and $L_{\text{Ly}\alpha} = 4 \times 10^{-24} n_e^2 f_{\text{v}} V \text{ erg s}^{-1}$ (e.g., McCarthy et al. 1990) assuming cylindrical symmetry and case B recombination. We have assumed a filling factor $f_{\text{v}} = 10^{-5}$, which is extremely uncertain (Heckman et al. 1982).

^eThe estimated $SFR \geq 8.12 \times 10^{-43} f_{\text{esc}}^{-1} L_{\text{Ly}\alpha}$ is very uncertain and based on the assumption that all of the Ly α flux is the result of Case B recombination of photoionization by a young stellar population (see Section 3.1).

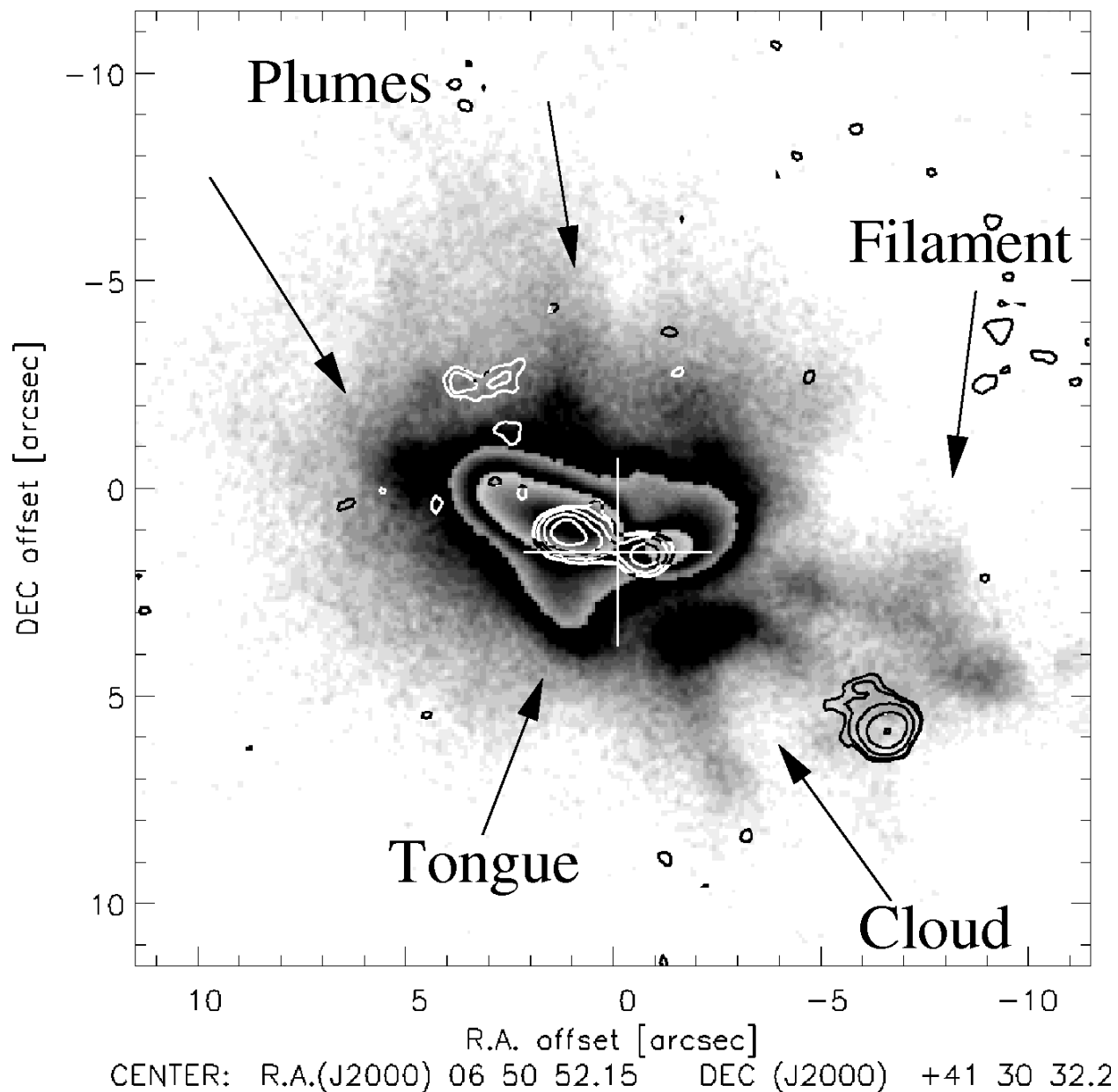


Fig. 1.— Grayscale Ly α image of 4C 41.17 with a contour representation of the 4.9 GHz VLA map (Carilli, Owen & Harris 1994) overlaid. The grayscale has been colorcycled to show the details of the high and low surface brightness simultaneously. The radio core is identified with a cross, and the contour levels are 0.07, 0.11, 0.4, 1.6 and 6.4 mJy beam $^{-1}$. The arrows indicate “plumes” of enhanced emission on both sides of the Northern Lobe, a separate emission line cloud with filaments extending to the SSW and SW, a large filament, and a Ly α tongue corresponding to a region which appears unaffected by the radio source.

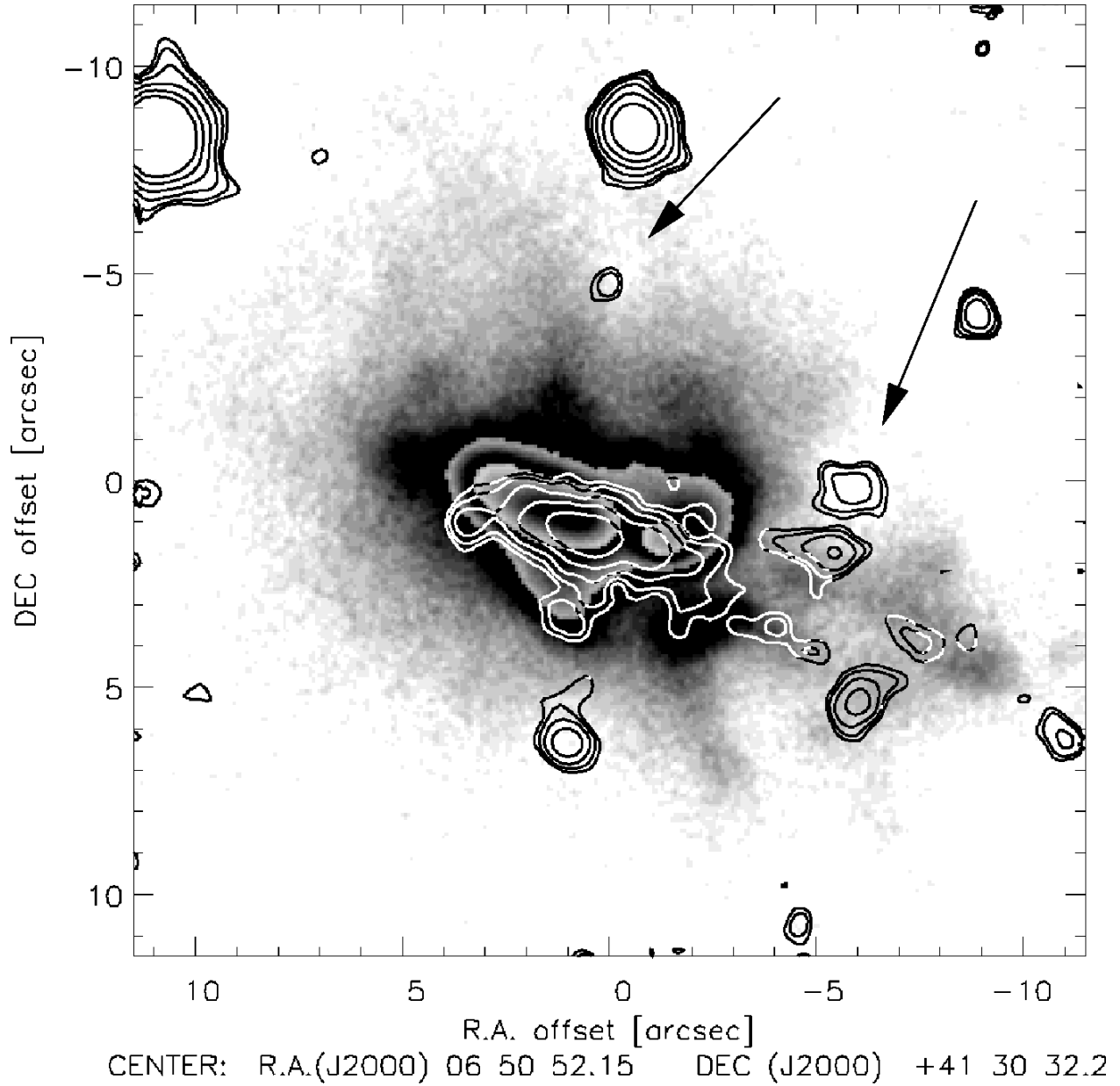


Fig. 2.— Similar to Figure 1 but with *K*-band image (contours; Graham et al. 1994) overlaid. The contours are at arbitrary levels and have been chosen to show the desired components. Some dips in the outer halo are co-spatial with *K*-band galaxies (indicated with arrows), suggesting that these galaxies are absorbing systems close in redshift to 4C 41.17.

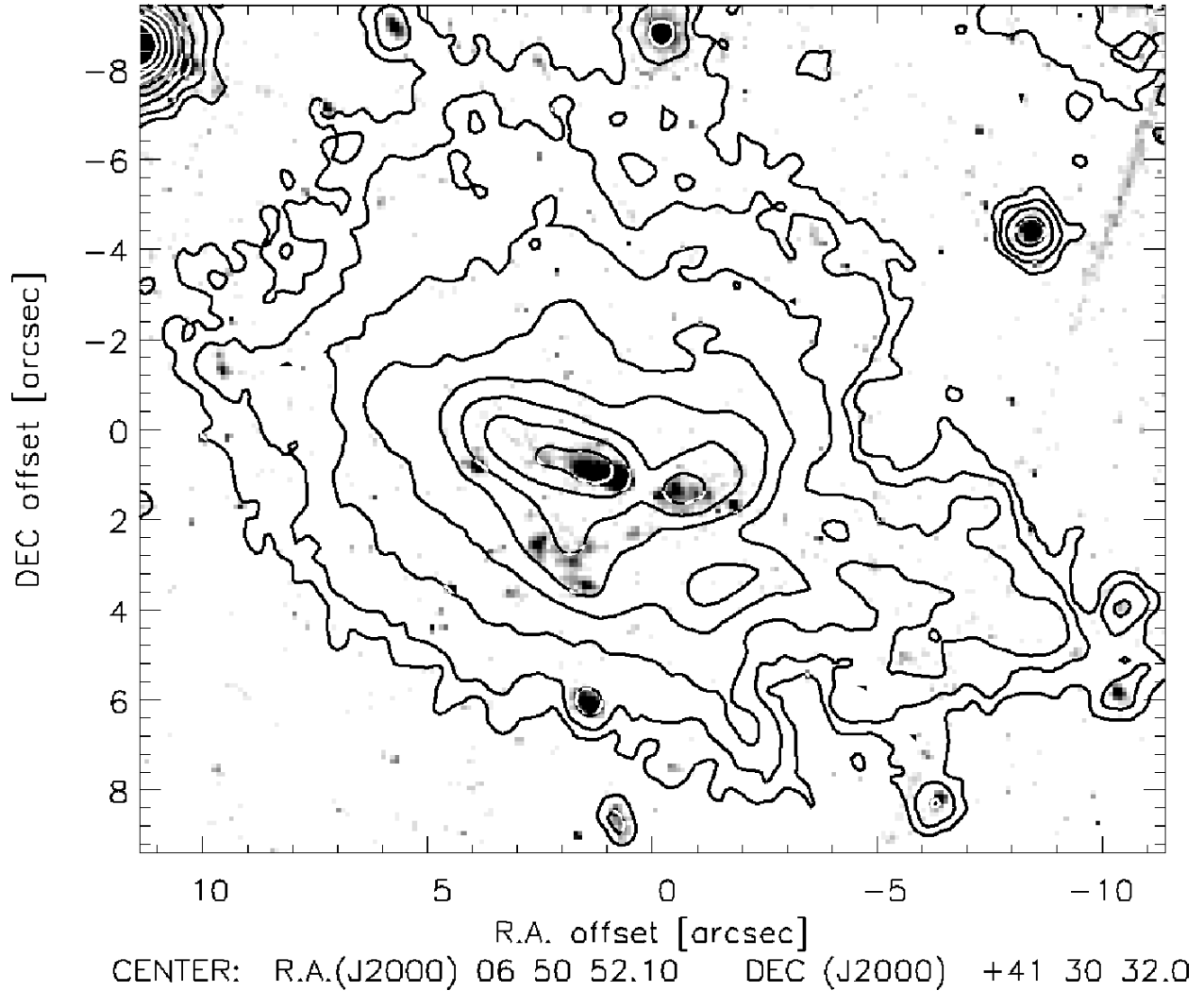


Fig. 3.— HST F702W image (van Breugel et al. 1999) of 4C 41.17 with narrow-band image (contours; including continuum) overlaid. The contours indicate observed surface brightness levels at $6.7 \times 10^{-19} \times (6, 12, 25, 50, 100, 200, 400, 800)$ ergs $^{-1}$ cm $^{-2}$ arcsec $^{-2}$. Note the group of kpc-sized clumps in the extended diffuse emission tongue 2'' south of the central peak, which is not aligned with the radio axis.

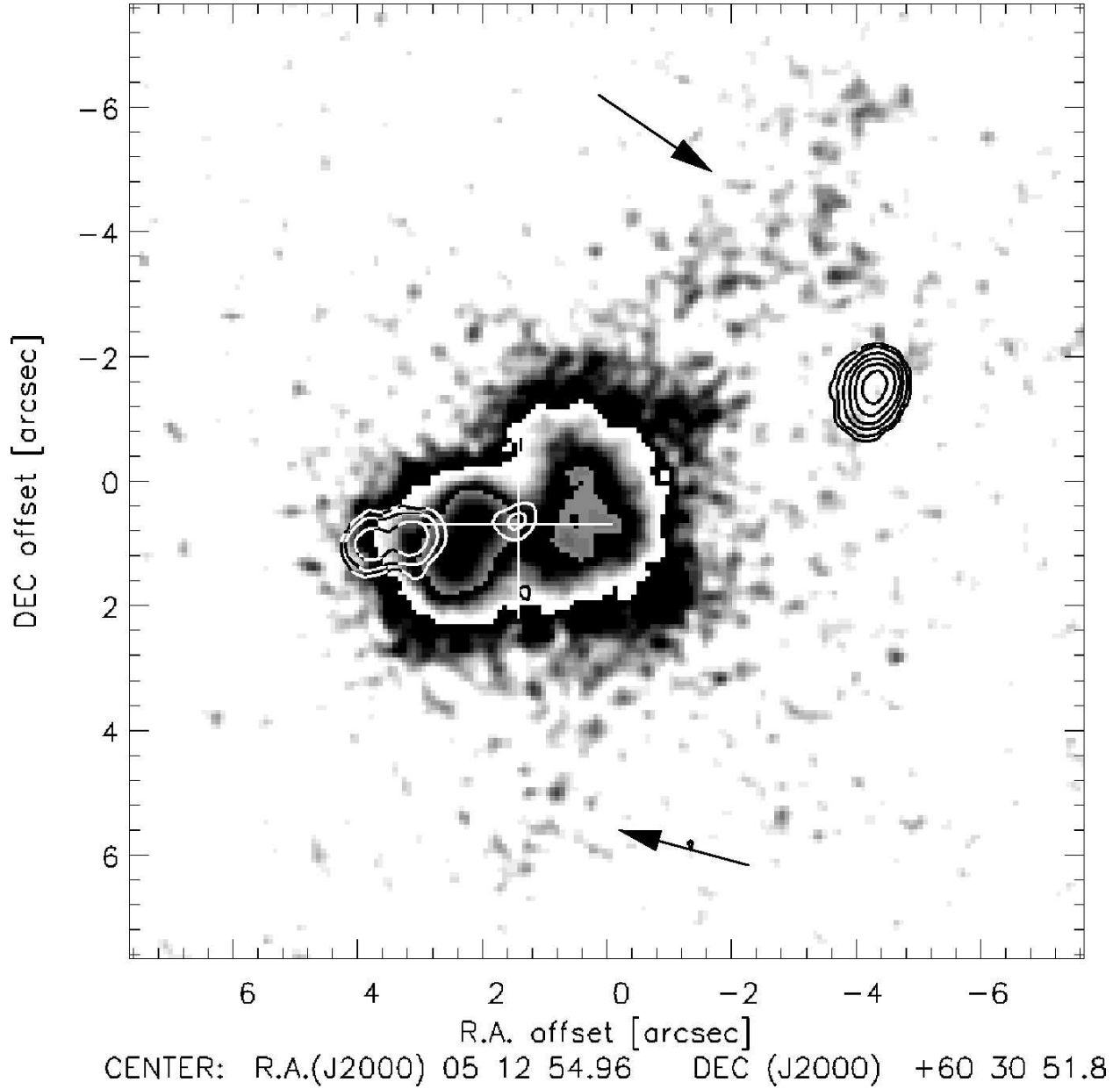


Fig. 4.— Ly α image of 4C 60.07 (grayscale) with 4.7 GHz VLA map (contours; Carilli et al. 1997) overlaid. The radio core is indicated with a cross, and the contour levels are 0.2, 0.4, 1.0, 2.0, 4.0 and 8.0 mJy beam⁻¹. A very extended NW filament and tentative evidence for a SE filament are indicated with arrows.

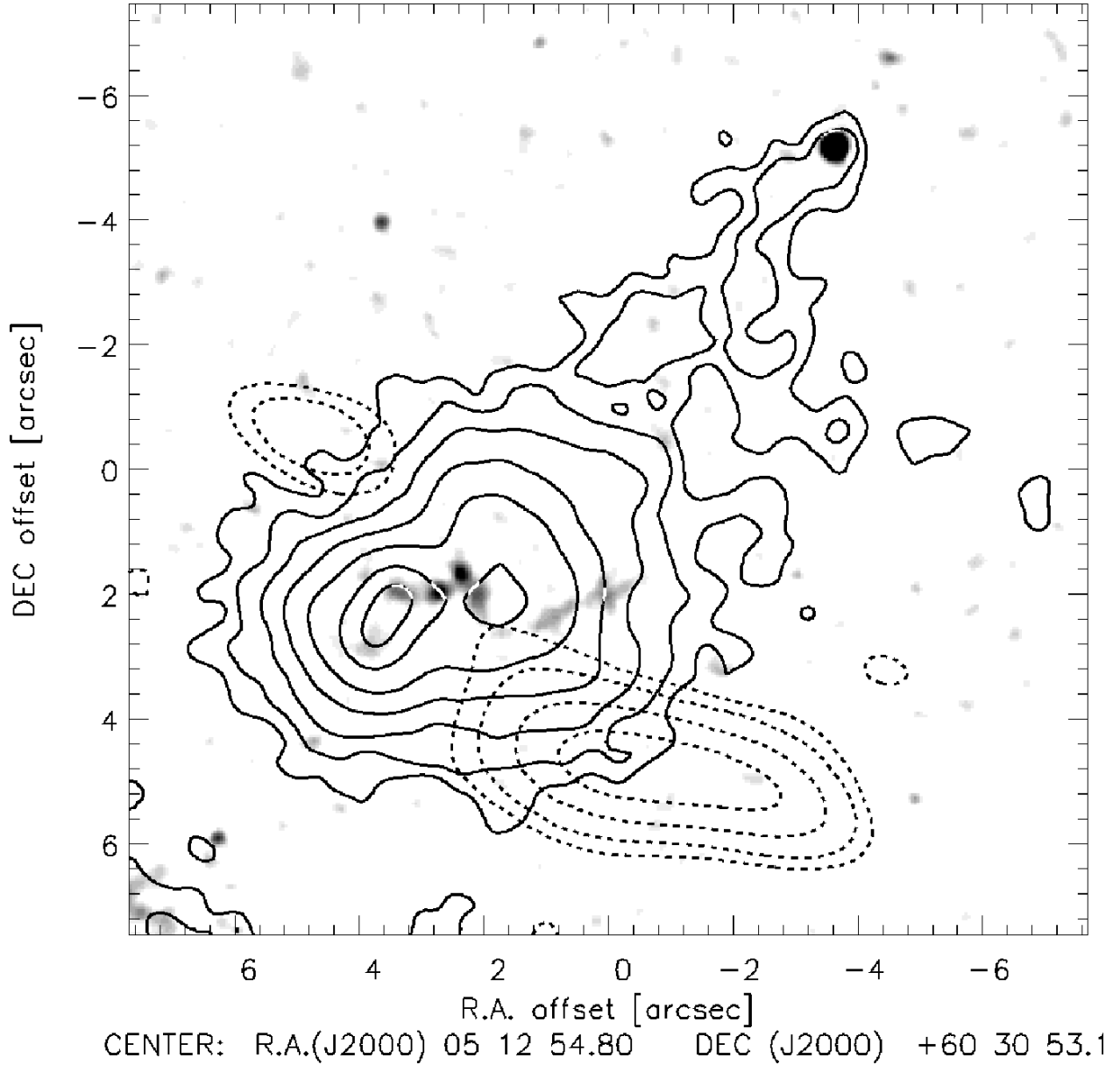


Fig. 5.— HST F702W image of 4C 60.07 with narrow-band image (solid contours, not extinction corrected, including continuum) and 1.25 mm map (dashed contours; Papadopoulos et al. 2000) overlaid. The narrow-band image has been heavily smoothed to bring out the low surface brightness filament and contour levels are $6.7 \times 10^{-19} \times (5, 10, 20, 40, 80, 160, 240) \text{ erg s}^{-1} \text{ cm}^{-2} \text{ arcsec}^{-2}$. The levels for the 1.25 mm emission are at 1.2, 1.6, 2.0, and 2.5 mJy, with $\sigma = 0.6 \text{ mJy beam}^{-1}$, showing that the NE component is a tentative detection comparable in size and shape to the restoring beam. The galaxy at the tip of the narrow-band filament is foreground at $z = 0.891$.

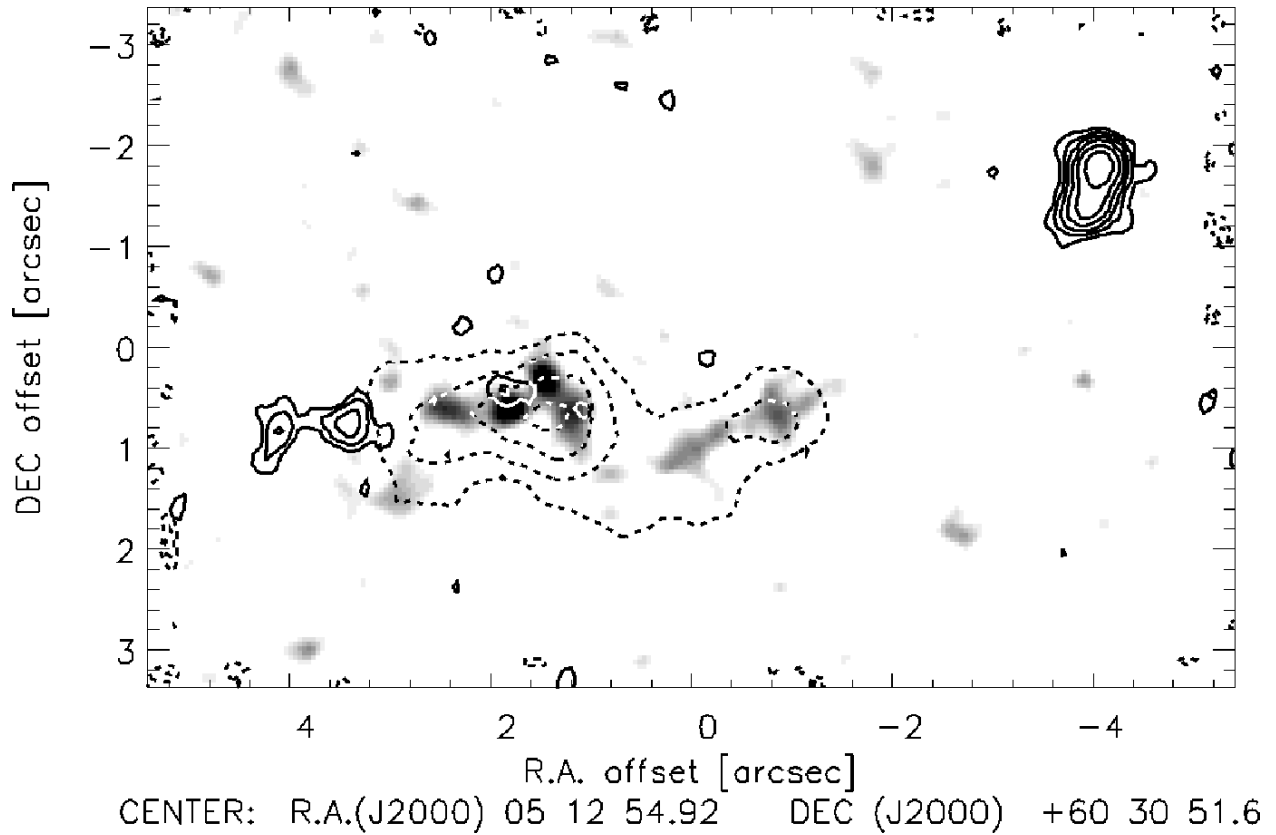


Fig. 6.— Zoomed in grayscale representation of the HST F702W image of 4C 60.07 with 8.2 GHz VLA map overlaid (solid contours; Carilli et al. 1997). The image has been smoothed to a resolution of $0.25''$, and ESI R -band contours (dashed) are overlaid to better show the shape of the galaxy. The knotty, Z-shaped structure of the aligned restframe UV continuum is apparent, while the radio core might be coincident with the central gap between the two brightest emission peaks. The radio contour levels are 0.08, 0.16, 0.3, 0.6, 1.2, and $2.4 \text{ mJy beam}^{-1}$.

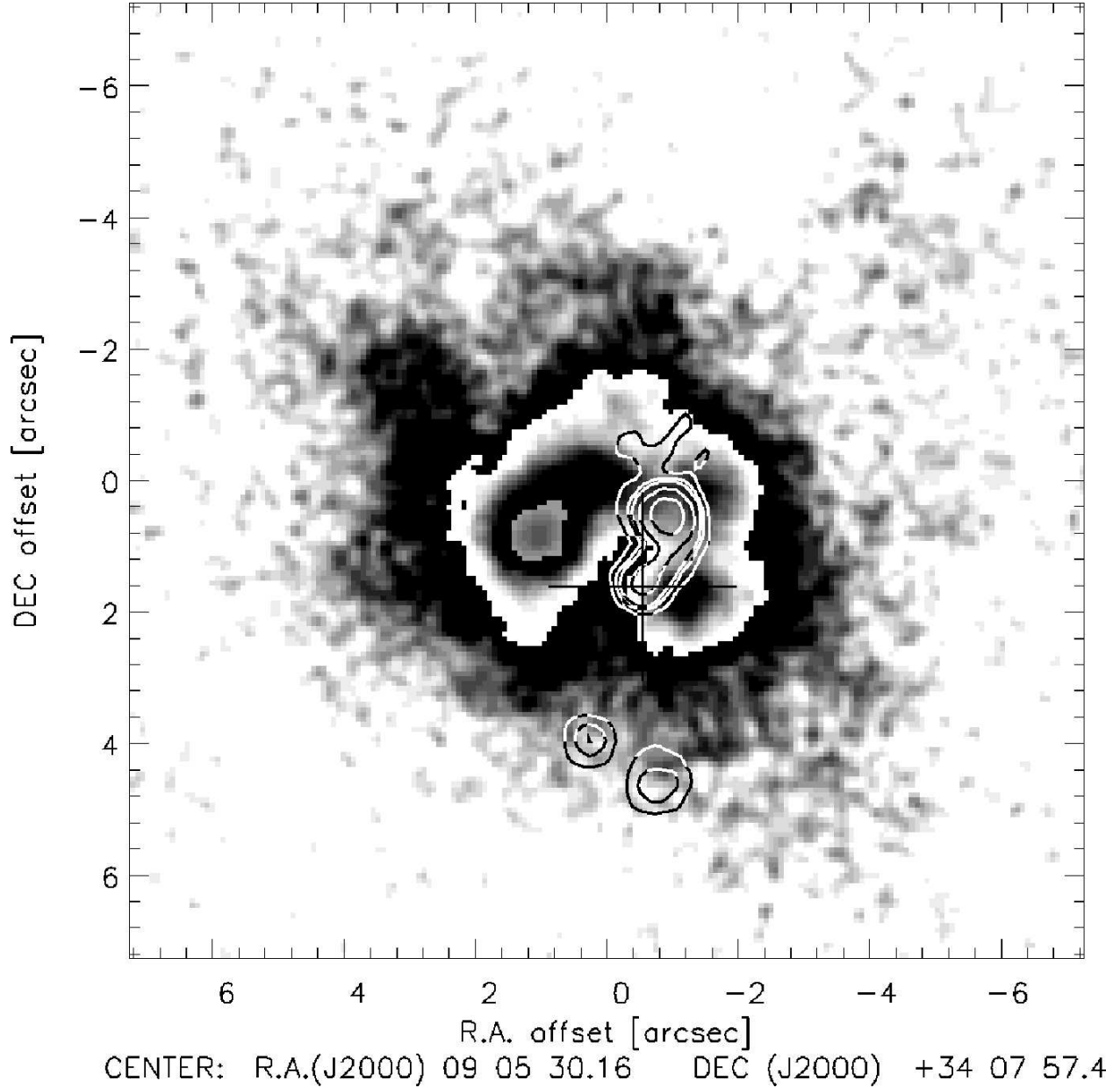


Fig. 7.— A continuum-subtracted Ly α image (grayscale) of B2 0902+34 with high resolution 4.9 GHz VLA radio map (contours; Carilli 1995) overlaid. The radio core is identified with a cross, and the contour levels are 0.2, 0.8, 1.6, 6.4, and 25.6 mJy beam⁻¹.

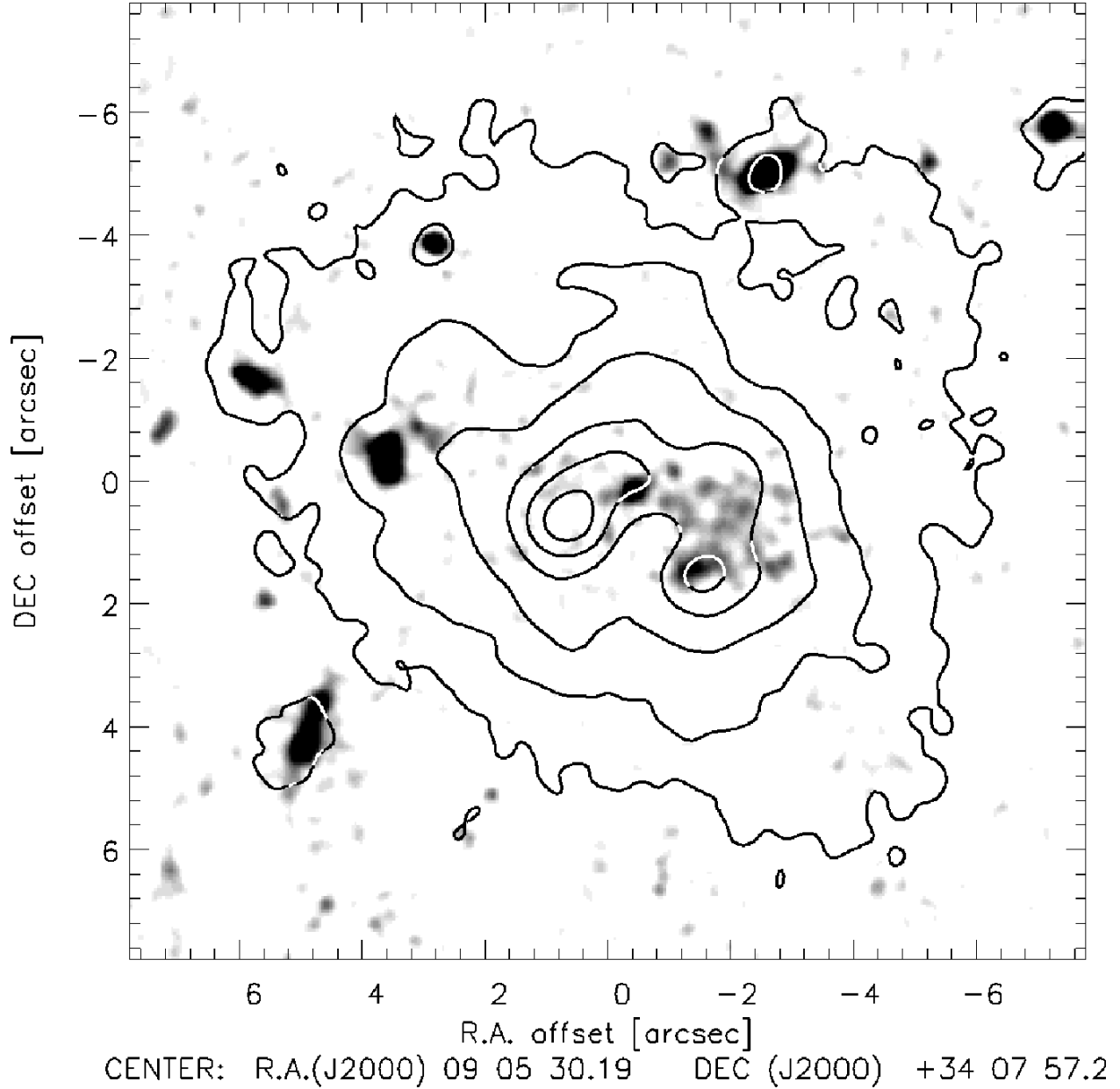


Fig. 8.— Narrow-band image contours of B2 0902+34 superposed on the HST F622W image. The contour levels are $8.4 \times 10^{-19} \times (8, 20, 40, 80, 120, 160)$ $\text{ergs}^{-1} \text{cm}^{-2} \text{arcsec}^{-2}$, include continuum emission, and have not been corrected for extinction.